Supporting Information

Multiple Effects Induced by Mo^{6+} Doping in $BiVO_4$ Photoanodes

*Annalisa Polo, Maria Vittoria Dozzi, Ivan Grigioni, Charles Lhermitte, Nukorn Plainpan, Luca Moretti, Giulio Cerullo, Kevin Sivula, and Elena Selli**

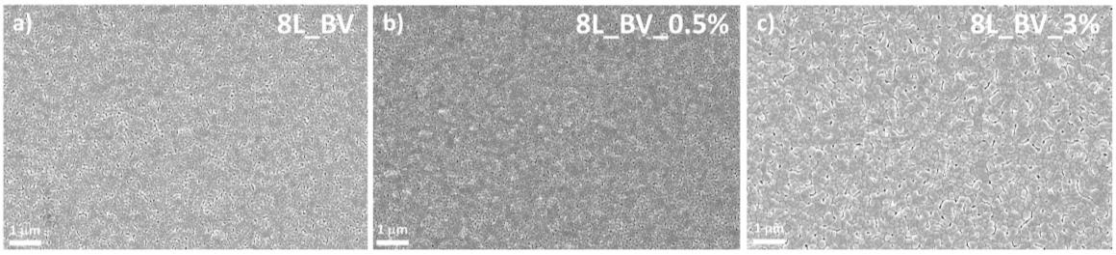

Figure S1. Top-down SEM images with low magnification (50.00 KX) of a) 8L_BV, b) 8L_BV_0.5% and c) 8L_BV_3%. The scale bar is 1 μm.

S1. Electrochemical Active Surface Area Determination

Many parameters describing the performance of electrodes (including the PEC performance) are referred to the geometric area of the irradiated spot of the electrode put in contact with the electrolyte. Nevertheless, the geometric area (A_g) is simply the projection on a plane (parallel to the macroscopic phase boundary of the electrode) of the real surface area (A) actually involved in any PEC process. These two entities are related each other by the linear relationship $A = A_g \cdot f_r$, where f_r is the roughness factor.[1]

Especially when comparing the activities of electrodes exhibiting substantial differences in morphology or structure, as in the case of the examined Mo^{6+} doped $BiVO_4$ (BV) photoanodes, the calculation of the real surface area is necessary for a correct interpretation of the observed results. An effective in situ approach to estimate the real surface area of the films is provided by the electrochemical active surface area (ECSA) obtainable from the capacitive current (*i.e.*, the non Faradic one) associated with the charging and discharging of the double layer built at the electrode/electrolyte interface.[1–3]

A valuable way to measure the capacitive current is through cyclic voltammetry (CV),[1] by properly selecting a narrow potential window (a few tens of millivolt), centred around the open circuit potential (OCP) of the investigated system, in which no Faradic process can take place. Under this hypothesis, the recorded current is only capacitive (I_c) and it depends linearly on the potential sweep rate (v) according to $I_c = C_{DL} \cdot v$, where C_{DL} represents the double layer capacitance of the interface and corresponds to the ECSA·C_s product, with C_s being the intrinsic specific capacitance of the semiconductor material (typically in the 15-130 μF cm^{-2} range[2]).

Such measurements were performed with the investigated electrodes in the dark, using the same cell configuration with a geometric area of 0.7 cm^2. For each of the tested electrodes, four consecutive CV traces, centred around the OCP and spanned over a narrow potential window (between –0.05 V and +0.05 V *vs.* OCP) were recorded at six different potential scan rates, ranging from 0.005 to 0.100 V s^{-1}, as shown in **Figure S2a** for the pure $BiVO_4$ electrode.

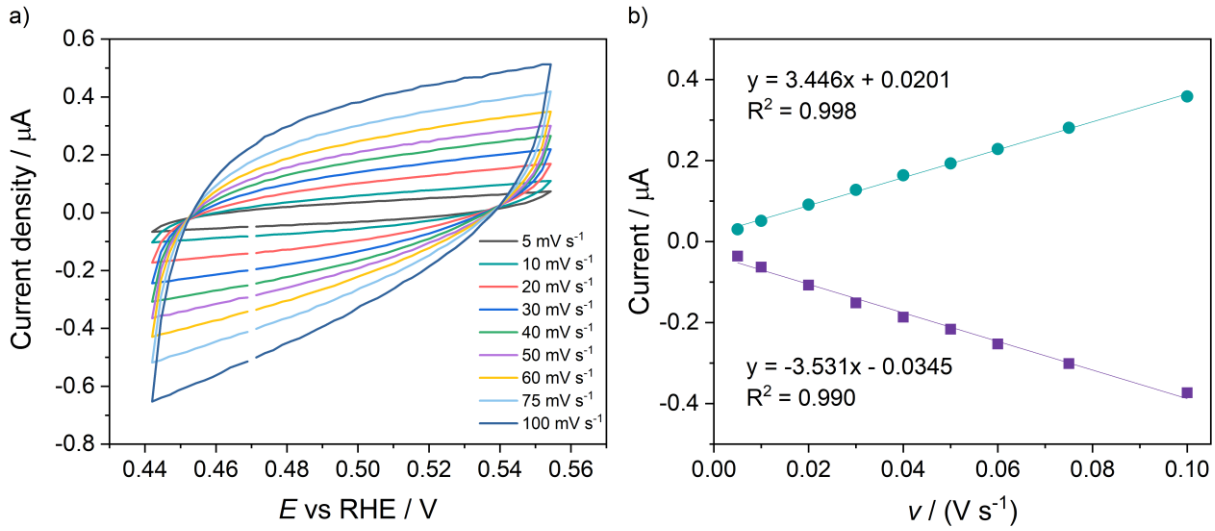

Figure S2. a) Cyclic voltammetry relative to the pure 8L_BV electrode recorded in the range between –0.05 and +0.05 V vs. OCP, at different potential scan rates (ranging from 0.005 to 0.100 V s^{-1}). b) Capacitive anodic and cathodic current values recorded with the 8L_BV electrode in a N_2-purged 0.5 M Na_2SO_4 solution, as a function of the potential scan rates (ranging from 0.005 to 0.100 V s^{-1}). The reported current values were extrapolated at the open circuit potential (OCP) value from the corresponding cyclic voltammetry scans recorded in the range between –0.05 and +0.05 V *vs.* OCP.

Unfortunately, the specific capacitance of $BiVO_4$ is not known in the open literature. Moreover, by considering that pretty low f_r can be obtained from these measurements by using

a C_s value of 60 μF cm^{-2} (as generally reported for metal oxides-based materials)[4] and that the actual determination of the absolute ECSA value for each electrode is out of our scope, *relative* ECSA values were determined for an internal comparison purpose, assuming that the small amount of added Mo^{6+} does not significantly affect the charging mechanism of the oxide material.

Relative ECSA values were thus obtained by evaluating the ratio between the C_{DL} slope attained with each electrode with respect to pure $BiVO_4$. In particular, such C_{DL} parameter is obtained as an average of the slopes (expressed in absolute value) obtained for the anodic and cathodic branches of the straight lines interpolating the recorded I_c values as a function of v, with I_c read in the middle of the CV potential window on the anodic and cathodic scan, respectively (see **Figure S2b**). The so obtained relative electrochemical active surface area values ($ECSA_{rel}$) are collected in **Table S1**.

Table S1. Relative electrochemical active surface area ($ECSA_{rel}$) values of the 4L, 6L and 8L electrodes, normalized with respect to that of the thinnest 4L_BV pure $BiVO_4$ electrode.

Electrode	4L	6L	8L
BV	1	0.9	0.9
BV_0.5%	1	0.8	0.6
BV_3%	0.7	0.5	0.3

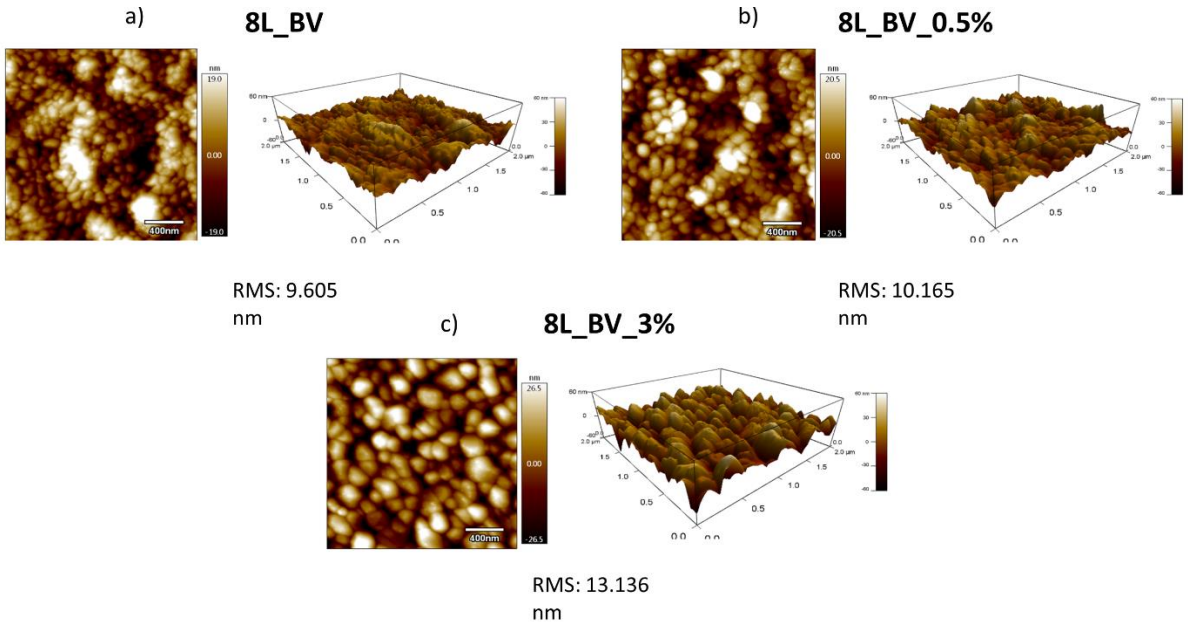

Figure S3. AFM images of a) 8L_BV, b) 8L_BV_0.5% and c) 8L_BV_3% films.

S2. Absorption Coefficients Determination

The absorption coefficient (α) for each electrode series was estimated on the basis of the Lambert-Beer law according to **Equation S1**, by considering the absorbance at 420 nm of the 8L thickest electrodes extracted from their absorption spectra (**Figure S4**) and the experimental thickness estimated from cross section images shown in **Figure 3**.

$$\alpha = \frac{1}{h} 2.303\ \mathrm{A} \qquad (S1)$$

where *h* is the thickness of the examined film and *A* is the absorbance at the specific wavelength. The so determined α values at 420 nm were 0.015 nm^{-1}, 0.020 nm^{-1} and 0.023 nm^{-1} for the pure BV, the 0.5 at% Mo^{6+} doped and the 3 at% Mo^{6+} doped films, respectively. The thickness of all the investigated photoanodes, estimated from the corresponding absorbance values at 420 nm, are collected in **Table S2**.

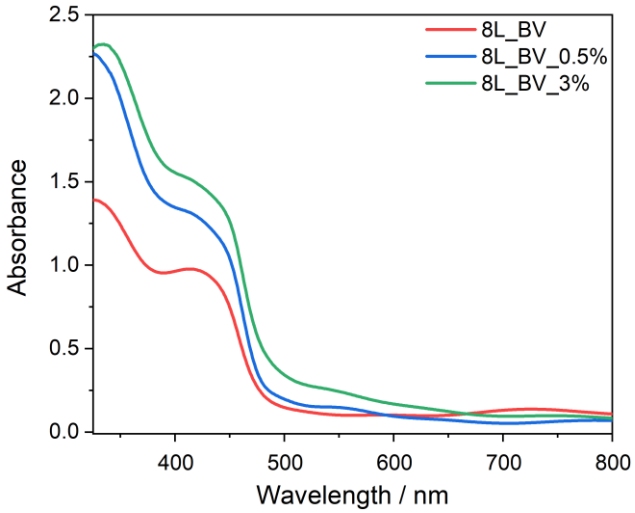

Figure S4. Absorption spectra (recorded in the transmittance mode) of the 8L_BV, 8L_BV_0.5% and 8L_BV_3% electrodes.

Table S2. Absorbance at 420 nm and estimated thickness of all film series.

	Absorbance at 420 nm			**Thickness / nm**		
Layers	BV	BV_0.5%	BV_3%	BV	BV_0.5%	BV_3%
1	0.12	0.27	0.18	19	32	18
2	0.37	0.44	0.51	57	52	51
3	0.40	0.67	0.73	62	79	73
4	0.60	0.80	0.88	92	95	88
6	0.83	1.10	1.34	128	129	134
8[†]	0.97	1.30	1.49	150	150	150

The thickness of the 8L_BV, 8L_BV_0.5% and 8L_BV_3% films were estimated from the cross section images reported in **Figure 3**.

Table S3. Penetration depths, ensuring 96%, 83% or 63% absorption of incident 420 nm light, estimated for the undoped and Mo-doped 8L films.

Material	**$\delta_{96\%}$/ nm**	**$\delta_{83\%}$ / nm**	**$\delta_{63\%}$ / nm**
8L_BV	200	134	67
8L_BV_0.5%	154	102	51
8L_BV_3%	130	87	43

S3. XPS Analysis after Etching

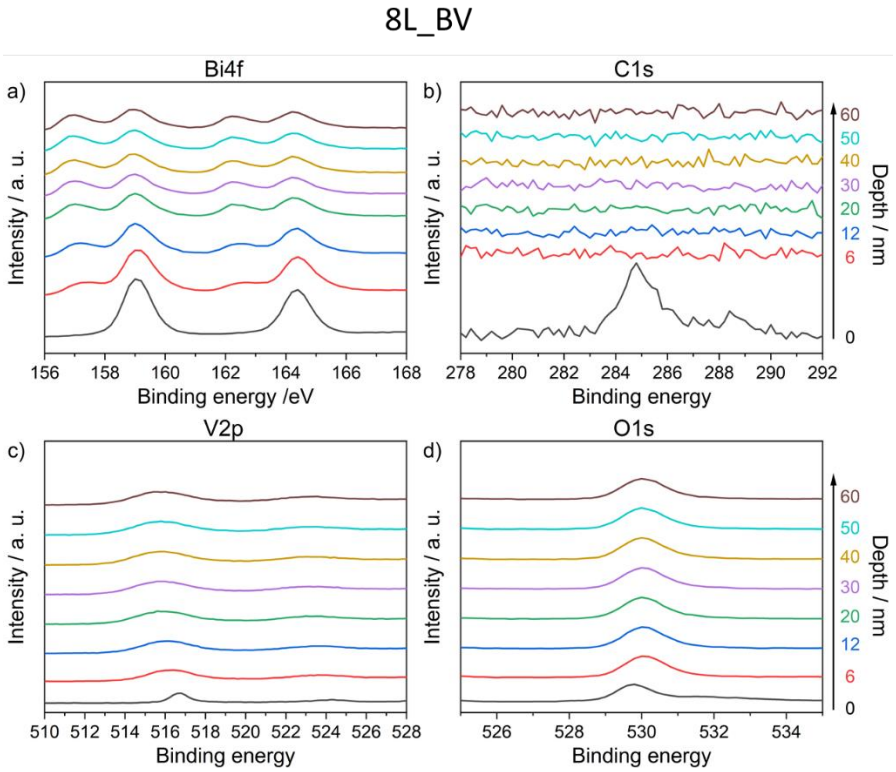

Figure S5. XPS spectra in the a) Bi 4f, b) C 1s, c) V 2p and d) O 1s binding energy region of 8L_BV, before (black line) and after Ar^+ ions sputtering at progressively increasing etching depth, in the 6 (red line) to 60 nm (brown line) range.

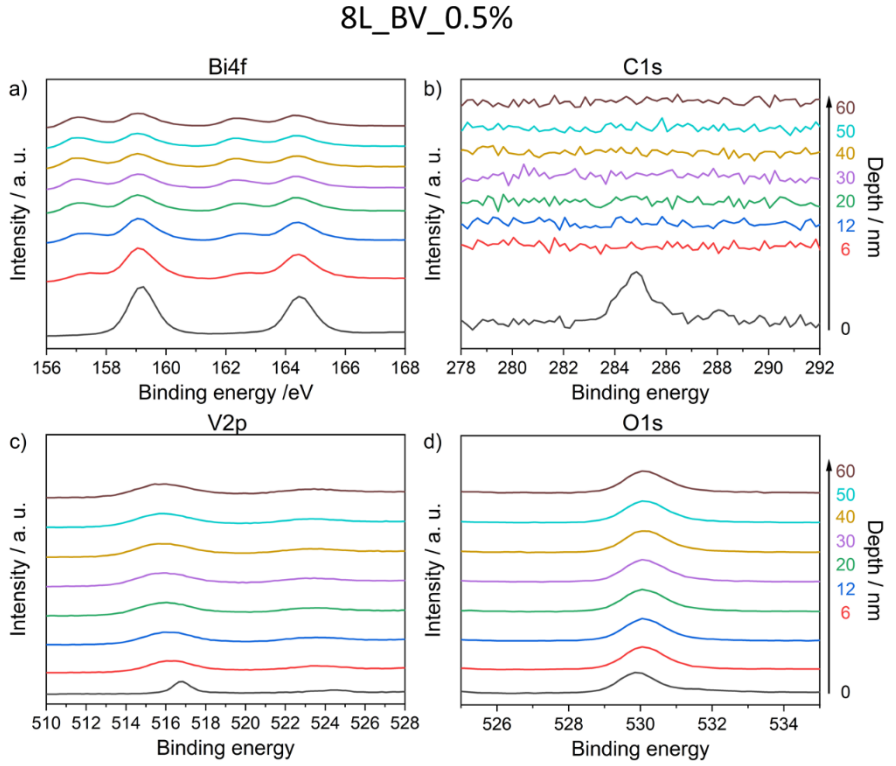

Figure S6. XPS spectra in the a) Bi 4f, b) C 1s, c) V 2p and d) O 1s binding energy region of 8L_BV_0.5%, before (black line) and after Ar^+ ions sputtering at progressively increasing etching depth, in the 6 (red line) to 60 nm (brown line) range.

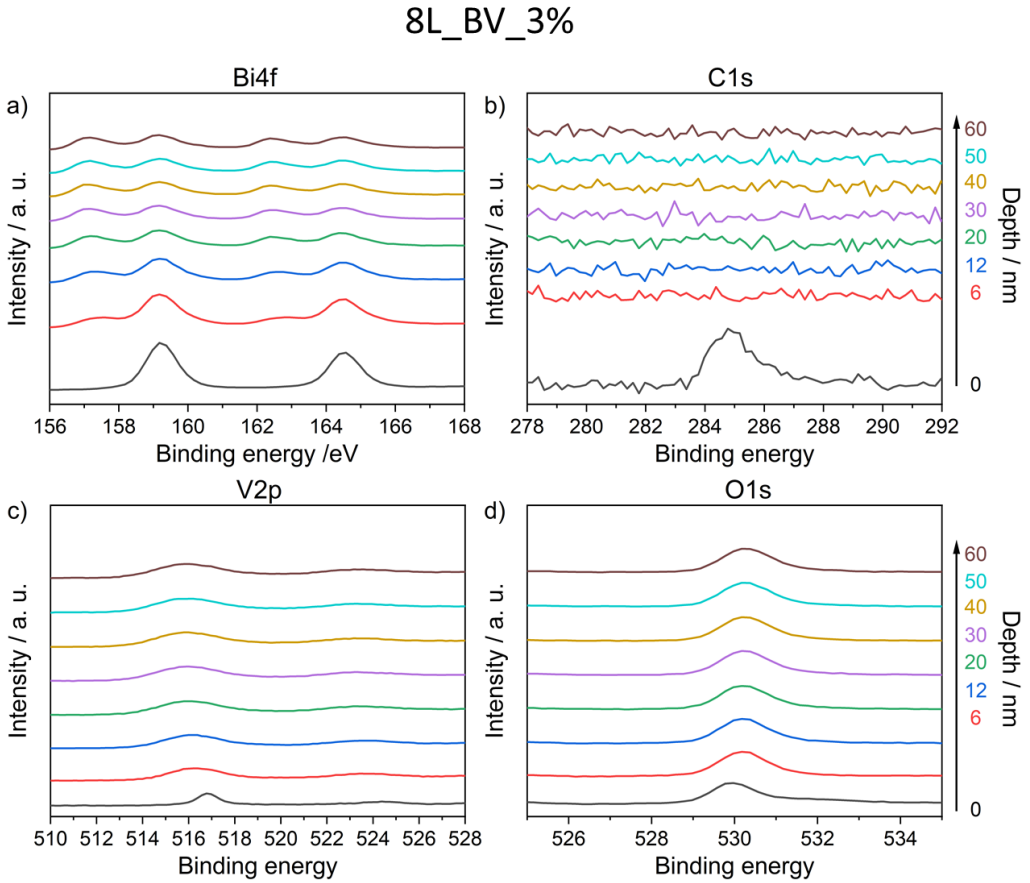

Figure S7. XPS spectra in the a) Bi 4f, b) C 1s, c) V 2p and d) O 1s binding energy region of 8L_BV_0.5%, before (black line) and after Ar^+ ions sputtering at progressively increasing etching depth, in the 6 (red line) to 60 nm (brown line) range.

Relative atomic ratios from XPS analyses of 8L films before and after etching.

	V:Bi	
Material	Surface	60 nm depth
BV	0.734	2.820
BV_Mo_0.5%	0.845	2.995
BV_Mo_3%	0.823	2.879

The V:Bi ratio is always lower than the expected 1:1 value, but it exceeds such value after etching (see Table above), in line with previous reports.[5,6] This may suggest that the investigated $BiVO_4$-based electrodes are characterized by non-stoichiometric, highly vanadium-deficient and bismuth-rich surfaces.

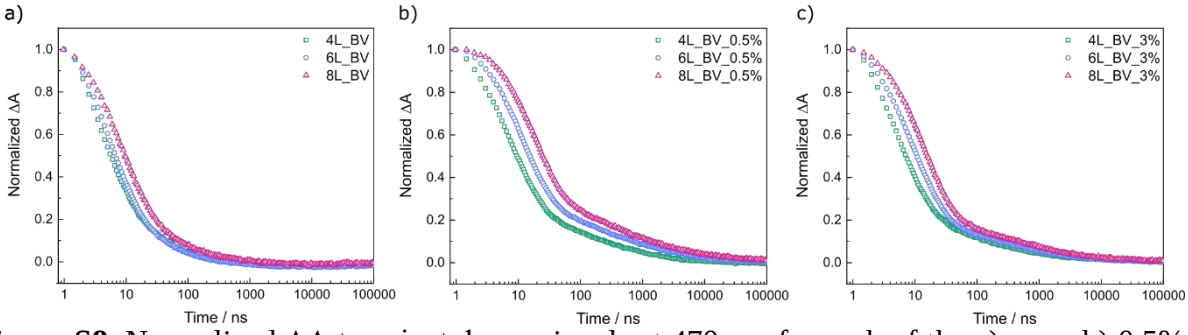

Figure S8. Normalized ΔA transient decay signals at 470 nm for each of the a) pure, b) 0.5% doped and c) 3% doped BV materials, on the overall 100 μs time scale.

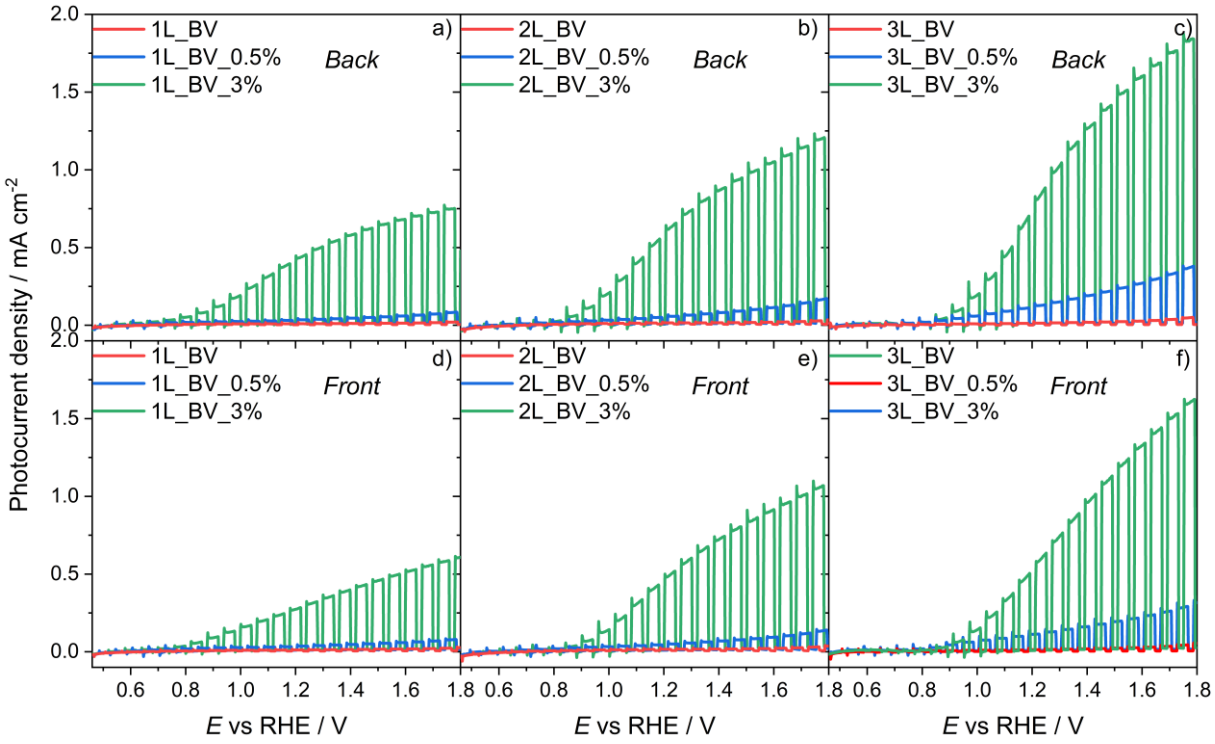

Figure S9. Linear sweep voltammetry (LSV) scans of the a,d) 1L, b,e) 2L and c,f) 3L films under a,b,c) back- and d,e,f) front-side irradiation in a 0.5 M Na_2SO_4 electrolyte solution.

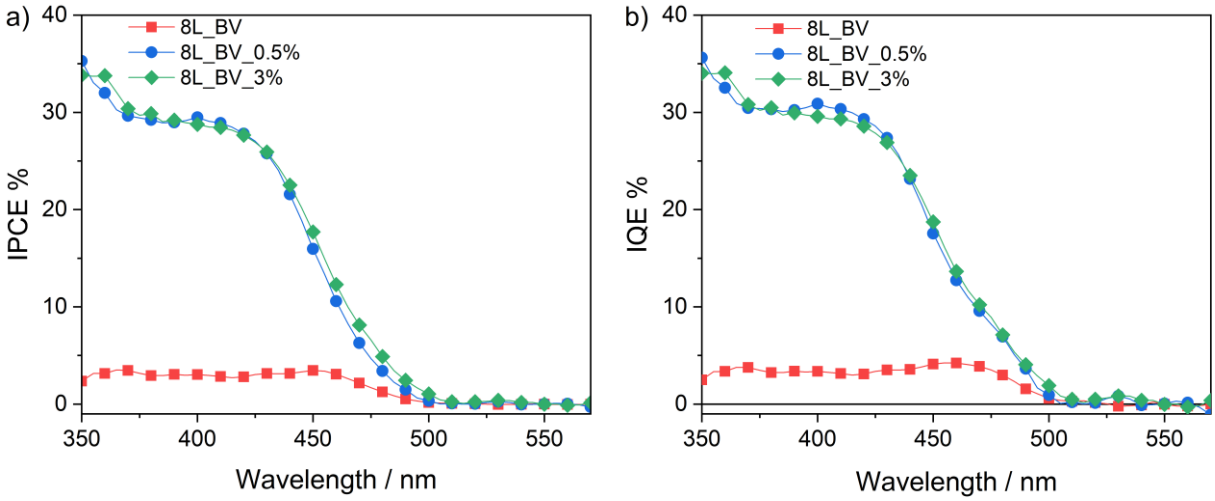

Figure S10. a) Incident photon to current efficiency (IPCE) and b) internal quantum efficiency (IQE) plots of the 8L photoanodes in a 0.5 M Na_2SO_4 electrolyte solution at 1.23 V *vs.* RHE, under front-side irradiation.

Table S4. Photocurrent density values (*J*) at 1.23 V *vs.* RHE obtained in LSV scans under AM 1.5 G solar simulated light in a 0.5 M Na_2SO_4 solution and from the integration of the IPCE values recorded in the same electrolyte solution over the solar spectral irradiance. Data refer to measurements performed under both back- and front-side irradiation.

	***J* from IPCE / mA cm^{-2}**		***J* under AM 1.5 G irradiation / mA cm^{-2}**	
Material	Back	Front	Back	Front
8L_BV	0.39	0.16	0.24	0.16
8L_BV_0.5%	0.37	1.14	0.31	0.72
8L_BV_3%	0.84	1.2	0.63	0.85

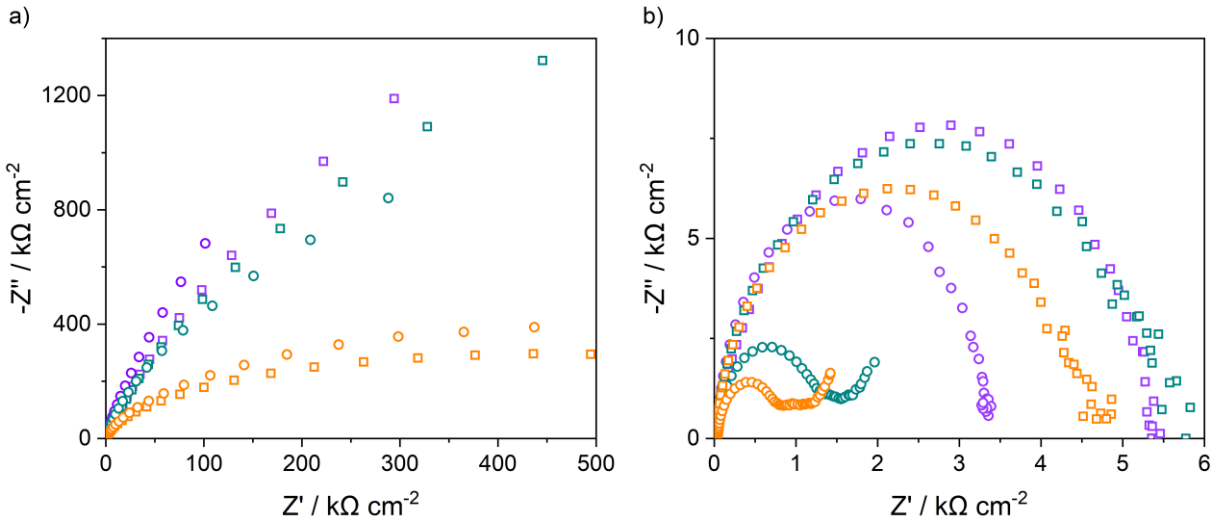

Figure S11. Nyquist plots obtained a) in the dark and b) under AM 1.5 G irradiation with the 8L_BV (squares) and the 8L_BV_3% electrode (circles) in a 0.5 M Na_2SO_4 solution, at 1.2 V (violet), 1.6 V (green) and 1.8 V (orange) *vs.* RHE.

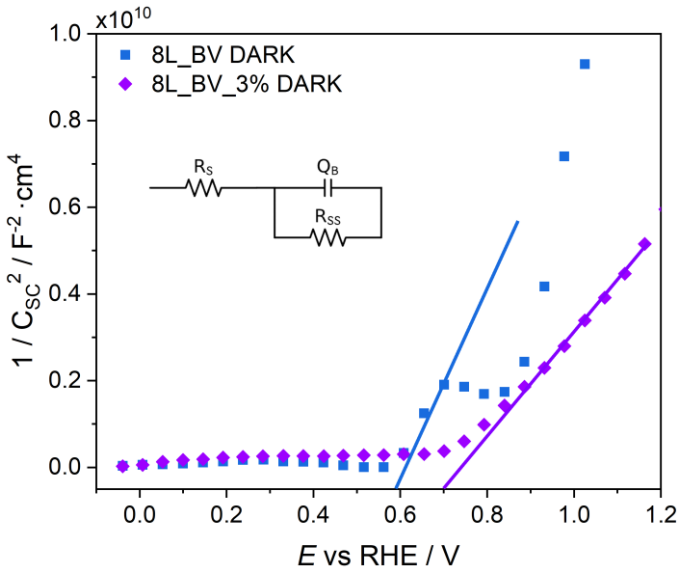

Figure S12. Mott-Schottky plots obtained in the dark with 8L_BV and 8L_BV_3% in contact with a 0.5 M Na_2SO_4 solution, and relative fitting lines. The inset shows the simple Randles model circuit employed.

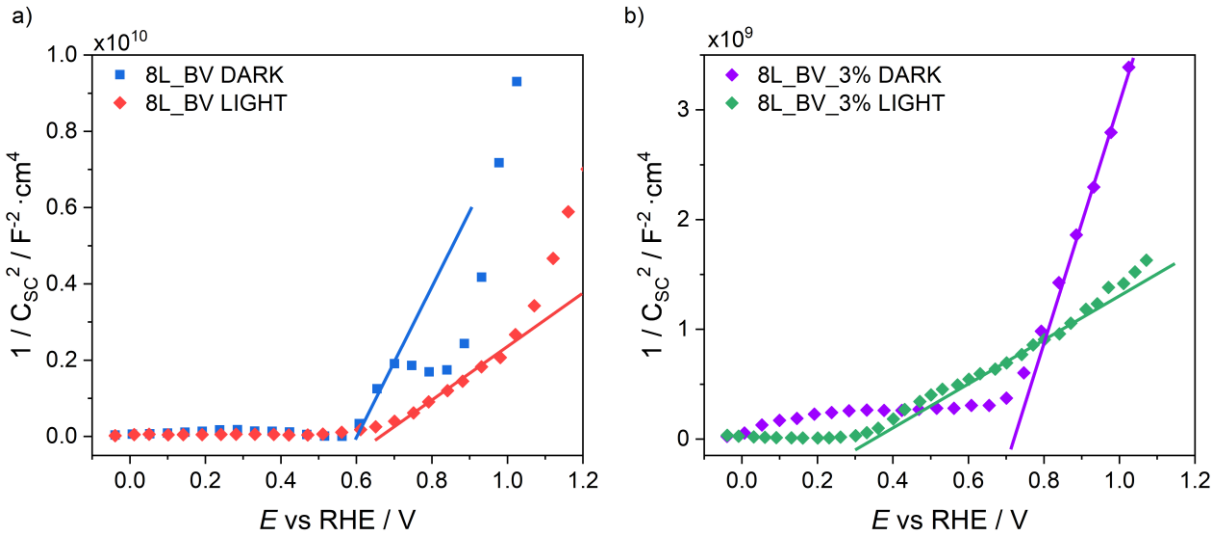

Figure S13. Mott-Schottky plots obtained in the dark and under AM 1.5 G irradiation with a) 8L_BV and b) 8L_BV_3% in contact with a 0.5 M Na_2SO_4 solution, and relative fitting lines.

[1] S. Trasatti, O. A. Petrii, *Pure Appl. Chem.* **1991**, *63*, 711.

[2] C. C. L. McCrory, S. Jung, J. C. Peters, T. F. Jaramillo, *J. Am. Chem. Soc.* **2013**, *135*, 16977.

[3] G. L. Chiarello, M. Bernareggi, M. Pedroni, M. Magni, S. M. Pietralunga, A. Tagliaferri, E. Vassallo, E. Selli, *J. Mater. Chem. A* **2017**, *5*, 12977.

[4] Q. Shi, S. Murcia-López, P. Tang, C. Flox, J. R. Morante, Z. Bian, H. Wang, T. Andreu, *ACS Catal.* **2018**, *8*, 3331.

[5] V. Nair, C. L. Perkins, Q. Lin, M. Law, *Energy Environ. Sci.* **2016**, *9*, 1412.

[6] W. Luo, Z. Li, T. Yu, Z. Zou, *J. Phys. Chem. C* **2012**, *116*, 5076.